Modelling interaction of multispecies plasmas with thermionic cathodes

To cite this article: M S Benilov *et al* 2005 *Plasma Sources Sci. Technol.* **14** 517

INSTITUTE OF PHYSICS PUBLISHING PLASMA SOURCES SCIENCE AND TECHNOLOGY

Plasma Sources Sci. Technol. **14** (2005) 517–524 doi:10.1088/0963-0252/14/3/014

Modelling interaction of multispecies plasmas with thermionic cathodes

M S Benilov[1], M D Cunha[1] and G V Naidis[2]

[1] Departamento de Física, Universidade da Madeira, Largo do Município, 9000 Funchal, Portugal
[2] Institute for High Temperatures of the Russian Academy of Sciences, Izhorskaya 13/19, Moscow 127412, Russia

Received 28 July 2004, in final form 6 May 2005
Published 9 June 2005
Online at stacks.iop.org/PSST/14/517

Abstract
The model of the near-cathode plasma, developed previously for the case of a single-species plasma-producing gas, is generalized for the case of multiple plasma-producing species. Results are presented of calculation of a diffuse mode of current transfer to tungsten cathodes in a mercury plasma with an addition of sodium. It is found that the presence of 1% of sodium results in a considerable expansion of the range of stability of the diffuse mode.

1. Introduction

The concept of nonlinear surface heating has become a widely accepted tool for modelling of current transfer to refractory cathodes of high-pressure arc discharges (e.g. [1–15]; see also reviews in [7, 16, 17]). In previous works the case of a single-species plasma-producing gas was dealt with.

A calculation of current transfer to thermionic cathodes in the framework of the concept of nonlinear surface heating consists of (a) a calculation of the near-cathode plasma layer and (b) a solution of the thermal conduction equation in the cathode body. The near-cathode layer of a plasma composed of atoms and ions of a single species and electrons can be calculated by means of the model developed in [18] and modified in [7, 9]. A theory of current transfer to a thermionic cathode, involving this model, has been validated by an extensive comparison with results of thermal and electrical measurements in the plasmas of inert gases [7, 19]. A brief summary of the theory is given in the appendix; a more detailed description and an online simulation tool based on this theory can be found on the internet [20].

In this paper, the model of the near-cathode plasma layer [7, 9, 18] is generalized to be applicable to a plasma composed of neutral particles and positive ions of several species, and electrons. The model thus obtained is employed for calculation of a diffuse discharge on tungsten cathodes in a mercury plasma with an addition of sodium. It is found that although the current–voltage characteristic of the near-cathode plasma region is not appreciably affected by the presence of sodium, stability of the diffuse mode may improve. This effect, deemed to be characteristic of the mixtures of gases with considerably different ionization energies, is studied in detail.

2. Generalizing the model of near-cathode layer to plasmas with multiple ion and neutral species

We need to apply the model of a near-cathode layer in a plasma composed of atoms and ions of a single species and electrons, developed in [7, 9, 18] and summarized in the appendix, to plasmas containing neutral particles and singly charged positive ions of several species and electrons. (Only singly charged ions are taken into account since they contribute dominantly to the total ion current to the cathode surface [21].) To this end, one should join all ion species into a single (effective) ion species and all neutral species into a single (effective) neutral species and introduce appropriate effective coefficients.

The procedure is as follows. The ion (or electron) number density $n_{i\infty}$ at the edge (on the plasma side) of the ionization layer, which appears in equations (11) and (13) of the appendix, is replaced by the combined density of all ion species at the edge of the ionization layer. The atomic number density $n_{a\infty}$ at the edge of the ionization layer, needed for evaluation of the coefficient C_2 appearing in equation (11), is replaced by the combined density of all neutral species at the edge of the ionization layer.

Effective coefficients to be introduced into the equations summarized in the appendix are the following: m_i the mass of the effective ion, m_a the mass of the effective neutral particle, Q_{ia} the average cross-section for momentum transfer in elastic collisions between the effective positive ion and the effective neutral particle, E the effective ionization energy (energy needed to produce an effective positive ion) and k_i the rate constant of ionization of the effective neutral particle

by electron impact. It is natural to evaluate these effective coefficients by means of averaging over all positive ion and/or neutral species:

$$m_\mathrm{i} = \sum_j aX_j m_\mathrm{i}^{(j)}, \quad m_\mathrm{a} = \sum_l bX_l m_\mathrm{a}^{(l)}, \quad E = \sum_j aX_j E^{(j)}, \tag{1}$$

$$Q_\mathrm{ia} = \sum_j aX_j \sum_l bX_l Q_{jl}, \quad k_\mathrm{i} = \sum_l bX_l k_\mathrm{i}^{(l)}, \tag{2}$$

where indices j and l are attributed to positive ions and to neutral species, respectively; $m_\mathrm{i}^{(j)}$ and X_j are the particle mass and the molar fraction of positive ions of a species j; $m_\mathrm{a}^{(l)}$ and X_l are the particle mass and the molar fraction of a neutral species l; Q_{jl} is the average cross-section for momentum transfer in elastic collisions between positive ions of a species j and neutral particles of a species l; $E^{(j)}$ is the energy needed to produce a positive ion of a species j (i.e. the ionization energy of the parent neutral particle); $k_\mathrm{i}^{(l)}$ is the rate constant of ionization of neutral particles of a species l by electron impact; $a = 1/\sum_j X_j$ and $b = 1/\sum_l X_l$ are normalization factors. Note that aX_j represents the fraction of a species j in the positive ion component of the plasma; bX_l represents the fraction of a species l in the neutral component of the plasma; the formula for Q_ia implies that the average value over neutral species is calculated for a fixed positive ion species, and this value is then averaged over all positive ion species.

Partial composition of the plasma is variable in the near-cathode plasma region, hence it is of interest to determine the point at which quantities aX_j and bX_l, appearing in equations (1) and (2), should be evaluated. We assume that these quantities are evaluated at the edge of the ionization layer, which seems to be the only practicable way to build a model of the near-cathode region without solving the differential equations describing the multi-component diffusion.

Thus, the problem of finding the densities of effective ion and neutral species and the effective coefficients may be solved in two steps. First, composition of the plasma at the edge of the ionization layer is determined by means of solving equations of local balance of production and loss of every plasma species in volume reactions for given elementary composition of the mixture and given values of the heavy-particle (gas) temperature T_h, electron temperature T_e and gas pressure p. After the equations governing plasma composition have been solved, one will be able to evaluate the densities of effective species $n_{\mathrm{i}\infty}$ and $n_{\mathrm{a}\infty}$ and the effective coefficients defined by equations (1) and (2).

In the case where the plasma consists of monatomic gases, the dominating mechanisms of ionization and recombination are usually ionization by electron impact and recombination with an electron being the third body. Then the above-mentioned equations of local balance coincide with the system of equations of ionization equilibrium (Saha equations) for each ion–atom pair, involving only the electron temperature T_e and not the heavy-particle temperature T_h. Hence, the plasma composition at the edge of the ionization layer may be found in this case by means of thermodynamic calculations, similarly to the case of an LTE plasma, $T_\mathrm{h} = T_\mathrm{e}$. If molecules are present, the contributions of electrons and heavy particles to some reactions may be comparable; e.g. this is the case of dissociation of halide molecules and recombination of metal and halogen atoms in metal halide plasmas. There is no detailed balancing between direct and reverse reactions in such cases, hence, kinetic data are required in addition to thermodynamic data.

3. Results for Hg–Na plasma

As an example, let us apply the model described in the preceding section to the case where the plasma-producing gas represents a mixture of mercury and sodium. Since ionization potentials of mercury and sodium are essentially different (10.44 eV and 5.14 eV, respectively), effects of the presence of multiple species are manifested in this case. Besides, this mixture is of interest in connection with high-pressure sodium lamps.

The rate constants of ionization of Na and Hg atoms by electron impact are calculated by adding rate constants of direct and stepwise ionization (e.g. [22]). The rate constants of stepwise ionization are evaluated by means of expressions given in [23] which are based on the modified diffusion approximation [22]. The rate constants of direct ionization of Na and Hg atoms are calculated, respectively, by means of approximations given in [23,24]. The effective rate constant of ionization of a neutral particle is shown in figure 1 as a function of T_e for various values of the molar fraction of sodium in the mixture, Z_Na. Also shown are ionization rate constants for the pure mercury and sodium plasmas. The plasma pressure was set equal to 5 bar, as well as in all the other calculations presented in this paper, and T_h was set equal to 3000 K. One can see that at high T_e the effective ionization rate constant in mixtures with small Z_Na is close to the ionization rate constant in the pure mercury plasma. At low T_e, the effective ionization rate constant in the mixtures is close to the product of Z_Na and of the ionization rate constant of sodium atoms (the contribution of ionization of mercury is small). This result has a clear physical explanation: at high T_e, the dominating ionization process is ionization of the most abundant atomic species (Hg); at low T_e, when ionization degrees of all atomic

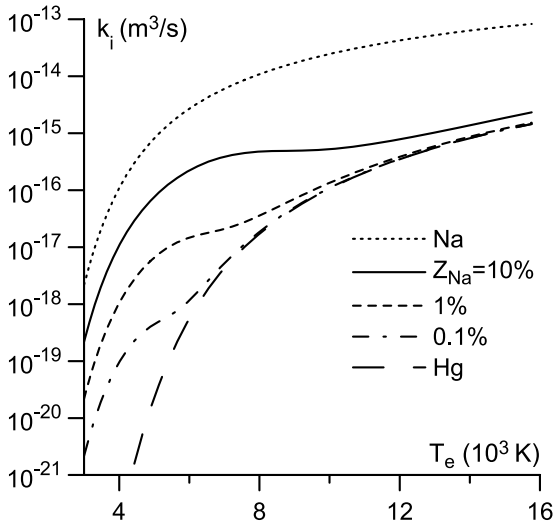

Figure 1. Effective ionization rate constant in the Hg–Na plasma, $T_\mathrm{h} = 3000$ K.

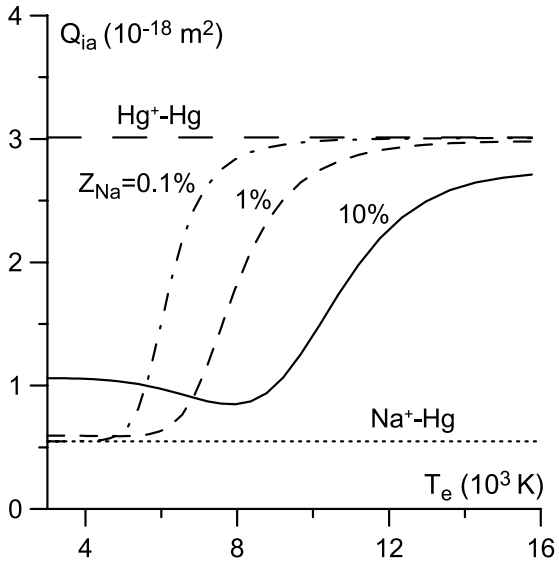

Figure 2. Effective average cross-section of momentum transfer in ion–atom collisions in the Hg–Na plasma, $T_h = 3000$ K.

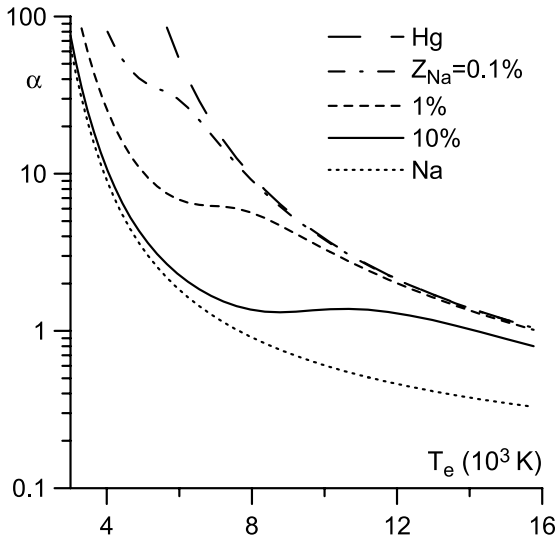

Figure 3. Ratio of the ionization length to the mean free path for ion–atom collisions, $T_h = 3000$ K.

species are small, the ionization of atoms with a low ionization potential (Na) dominates.

Data on individual momentum transfer cross-sections Na^+–Na, Na^+–Hg, Hg^+–Na and Hg^+–Hg are required for a calculation of the effective average ion–atom momentum transfer cross-section Q_{ia}. The cross-sections Na^+–Hg and Hg^+–Na are governed by the polarization interaction, while the cross-sections Na^+–Na and Hg^+–Hg are governed by the charge transfer process. The effective average cross-section Q_{ia} is shown in figure 2. Also shown are the average cross-sections of momentum transfer in Na^+–Hg and Hg^+–Hg collisions. It is seen that the change in ion composition takes place in the range of T_e approximately (6–12) $\times 10^3$ K. Note that there is a difference between the effective cross-section and the cross-section of Na^+–Hg collisions at low T_e in the case $Z_{Na} = 10\%$, which is because of the presence of sodium atoms in the mixture, in addition to the atoms of mercury.

An important parameter governing the physics of the near-cathode plasma layer is α, the ratio of the ionization length to the mean free path for ion–atom collisions; see equation (12) in the appendix. This ratio for various values of Z_{Na} is shown in figure 3. Shown also are values of this ratio for the pure mercury and sodium plasmas. One can see that in the electron temperature range (5–10) $\times 10^3$ K, typical of the diffuse mode of cathode operation, values of α in a Hg–Na plasma with $Z_{Na} \gtrsim 1\%$ are substantially smaller than those in the pure mercury plasma and are of the order of unity rather than large. It means that the use of the diffusion description of the ionization layer would be unjustified and the use of the fluid description (in which equation (11) of the appendix originates) is especially important under these conditions.

The density of the energy flux from the Hg–Na plasma to the cathode surface for several Z_{Na} values is shown in figure 4(*a*) in a wide range of surface temperature values and in figures 4(*b*) and (*c*) for a narrow surface temperature range around 3000 K which is typical of the diffuse mode. (In order to give an idea of conditions typical of the diffuse mode, we note that the energy flux density needed to heat a tungsten cathode of a height of the order of 20 mm up to temperatures of about 3000 K is of the order of 10^7 W m^{-2}.) All the calculations described in this paper have been performed for a tungsten cathode, as well. The work function of the cathode surface was set equal to 4.55 eV which is the value corresponding to pure tungsten; the effect of variation of the work function owing to formation of an alkali metal monolayer on the cathode surface is treated elsewhere [25] (see also a comment at the end of the next section). The energy flux from the pure mercury and pure sodium plasmas is also shown.

On the scale of figure 4(*a*), the difference between the data for the Hg–Na and pure mercury plasmas is minor. Consequently there will be no major difference between the thermal regimes of cathode spots in a Hg–Na plasma with $Z_{Na} \lesssim 1\%$ and the pure mercury plasma. However, the difference at low temperatures (figures 4(*b*) and (*c*)) is considerable, which indicates a possible difference in characteristics of the diffuse mode of cathode operation. One can see, from figures 4(*b*) and (*c*), that the energy flux from the Hg–Na plasma at Z_{Na} of the order of 1% at low temperatures of the cathode surface is close to that of the pure sodium plasma and approaches the energy flux from the pure mercury plasma at high temperatures. Given that the electron temperature increases with an increase in temperature of the cathode surface, this behaviour is consistent with that shown in figures 1 and 2.

The current–voltage characteristic $U(I)$ of a tungsten cathode of radius $R = 1$ mm and of height $h = 14.5$ mm in a Hg–Na plasma with $Z_{Na} = 1\%$ is shown in figure 5. (Here U is the near-cathode voltage drop and I is the arc current.) Also shown are characteristics for the pure mercury, sodium and argon plasmas. As far as the pure plasma-producing gases are concerned, a clear tendency is present: a decrease in the ionization potential results in a decrease of the voltage necessary for maintaining a given current. In the case of the Hg–Na plasma, the current–voltage characteristic is close to that for the case of pure sodium plasma at low currents and approaches the current–voltage characteristic of

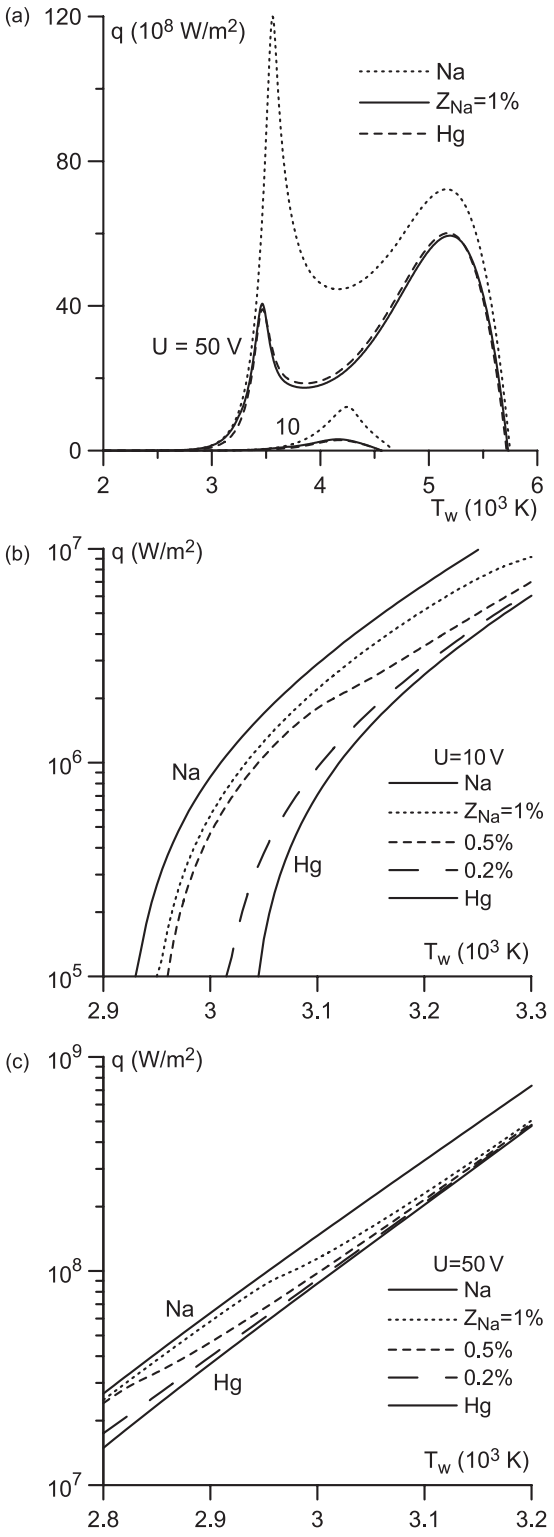

Figure 4. Energy flux from the plasma to the surface of a tungsten cathode.

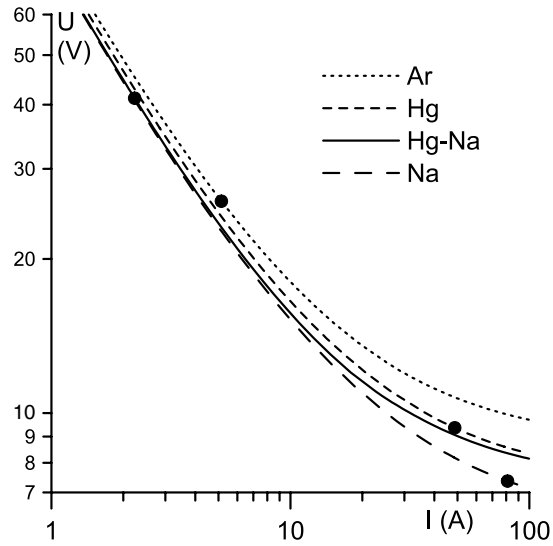

Figure 5. Current–voltage characteristics and stability limit of the diffuse mode.

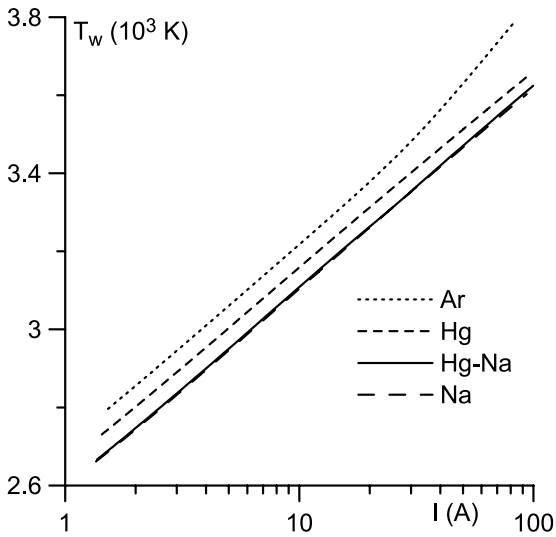

Figure 6. Maximum temperature of the cathode surface in the diffuse mode.

the pure mercury plasma at high currents. Given that the electron temperature increases with an increase of current, this behaviour is consistent with that shown in figures 1 and 2.

The maximum temperature of the cathode surface (which is attained at the edge of the front surface [7]) evaluated for the conditions of figure 5 is shown in figure 6. In the case of pure plasma-producing gases, a decrease of the ionization potential results in a weak decrease of the cathode surface temperature at a fixed current. The maximum temperature in the case of the Hg–Na plasma is close to that in the case of the pure sodium plasma.

At high arc currents, the diffuse mode of current transfer is stable. As the current decreases, the diffuse mode becomes unstable and a transition to the spot mode occurs. The results of experimental investigations of this transition can be found, e.g. in [26] (see also references therein). A theoretical description of this transition has been developed in [1, 9]. This transition was treated in [1, 9] as a manifestation of an instability of thermal balance of a body heated by a nonlinear external energy flux and the limit of stability of the diffuse mode was calculated (i.e. the current value at which the diffuse mode is neutrally stable; this value separates regions of stability

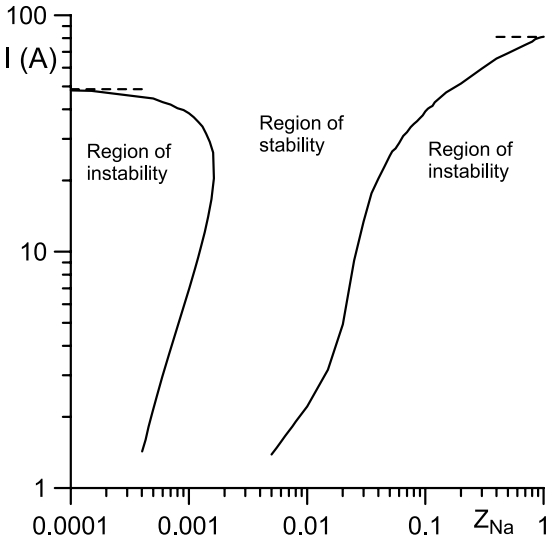

Figure 7. Regions of stability and instability of the diffuse mode in the Hg–Na plasma for variable plasma composition. - - - -: stability limits for the pure mercury and sodium plasmas.

and instability). The results of the calculation of the limit of stability are depicted by points in figure 5. As far as the pure plasma-producing gases are concerned, a clear tendency is present: as the ionization potential decreases, the region of instability of the diffuse mode expands to higher currents. This tendency conforms to previous simulations [9] and to the experiment [27]. However, it is violated in the case of the Hg–Na plasma, where the stability limit is lower than that in both mercury and sodium (in fact, it is even lower than that in the argon plasma). In other words, an addition of 1% of sodium to mercury results in a considerable expansion of the range of stability of the diffuse mode.

In figure 7, regions of stability and instability of the diffuse mode on a tungsten cathode of radius $R = 1$ mm and of height $h = 14.5$ mm in a Hg–Na plasma are shown as functions of Z_{Na}. Note that at each Z_{Na} close to 10^{-3} the criterion of neutral stability [9] is satisfied at two different current values. For example, at $Z_{Na} = 10^{-3}$ it is satisfied at $I_1 \approx 38.5$ and at $I_2 \approx 7.0$ A. One can hypothesize, in such situations, that the diffuse mode is stable at $I > I_1$, is unstable at $I_2 < I < I_1$ and regains stability (at least, with respect to the first-mode three-dimensional perturbations) at $I < I_2$.

One can see from figure 7 that at $Z_{Na} \lesssim 10^{-4}$ and $Z_{Na} \gtrsim 0.1$ the limit of stability in the Hg–Na mixture is close to that in either pure mercury or pure sodium. There is a dramatic extension of the stability region at intermediate Z_{Na}. (In fact, there is a certain range of Z_{Na}, $1.6 \times 10^{-3} \lesssim Z_{Na} \lesssim 5 \times 10^{3}$, in which the instability disappears completely, i.e. the diffuse mode becomes stable against the first mode of three-dimensional perturbations in the current range considered.) The reason for this extension is that the stability of the diffuse mode is governed by the derivative $\partial q/\partial T_w$ evaluated at constant U [1] and that lower values of this derivative favour stability. One can see from figures 4(*b*) and (*c*), that there is a pronounced decrease of this derivative in the range of T_w typical of the diffuse mode for a Hg–Na plasma at Z_{Na} of the order of 1% (this decrease is due to the energy flux from the Hg–Na plasma at Z_{Na} of the order of 1% at low temperatures being close to that from the pure sodium plasma and approaching the energy flux from the pure mercury plasma at high temperatures). It is this decrease of the derivative $\partial q/\partial T_w$ that causes the extension of the stability region.

4. Concluding remarks

The model of the near-cathode plasma [7, 9, 18], developed previously and validated by the experiment for the case of a single-species plasma-producing gas, has been generalized for the case of multiple ion and multiple neutral species and used for calculation of a diffuse mode of current transfer to tungsten cathodes in a mercury plasma with an addition of sodium. It is seen that the presence of 1% of sodium, while not strongly affecting the characteristics of the diffuse mode (such as the current–voltage characteristic of the near-cathode plasma region and the maximum temperature of the cathode surface), results in a considerable expansion of the range of stability of the diffuse mode. The latter effect occurs because the dominating ionization process at high T_e is ionization of the most abundant atomic species (Hg) while at low T_e the ionization of atoms with a low ionization potential (Na) comes into play. One can expect that this effect is characteristic of all mixtures of gases with substantially different ionization energies.

Addition of alkali metals like sodium affects the current transfer to thermionic cathodes in two ways: through the variation of properties of the near-cathode plasma layer owing to the presence of metal atoms in the gas phase and through the variation of the work function of the cathode surface owing to formation of an alkali metal monolayer on the surface. Only the first effect is studied in this work; i.e. all the calculations have been performed for a fixed work function of the cathode material. Effects caused by a variation of the work function of the cathode surface owing to formation of a monolayer of alkali metal atoms on the surface are studied in [25]. It is shown that in the case of the Na–Hg plasma, formation of the sodium monolayer affects the diffuse mode of current transfer only moderately and in the same direction of metal atoms in the gas phase, i.e. the cathode surface temperature and the near-cathode voltage drop decrease weakly while the range of stability of the diffuse mode expands. In other cases, the effect of an alkali monolayer may be dramatic, as shown in the example of Cs–Hg plasma.

Acknowledgments

The work was performed within activities of the project *NumeLiTe* of the 5th Framework programme ENERGIE of the EC, of the project POCTI/FIS/60526/2004 of FCT and FEDER, and of the action 529 of the programme COST of the EC.

Appendix A. Model of interaction of thermionic cathodes with high-pressure plasmas produced in pure monoatomic gases

In this appendix, a summary of equations of the theory of interaction of thermionic cathodes with high-pressure plasmas

composed of atoms of a single species, ions of a single species and electrons is given. A more detailed description and an online tool for simulation of the diffuse mode of current transfer based on this theory can be found in [20]. Detailed presentations of different aspects of the theory can be found in the original works cited below.

Appendix A.1. Model of nonlinear surface heating

Let us consider a thermionic cathode of a high-pressure arc discharge. Joule heat generation inside the cathode body is assumed to be negligible, and the thermal conductivity κ of the cathode material is assumed to be a known function of its temperature: $\kappa = \kappa(T)$. The base of the cathode is maintained at a fixed temperature T_c by external cooling and the rest of the cathode surface is in contact with the plasma or the cold gas and is heated or cooled, respectively.

A steady-state temperature distribution in the cathode body is governed by the equation of thermal conduction

$$\nabla \cdot (\kappa \nabla T) = 0. \tag{3}$$

The boundary condition at the base of the cathode reads

$$T = T_c. \tag{4}$$

The density q of the net energy flux from the plasma or the cold gas to the cathode surface is evaluated as the difference between the density of the energy flux from the plasma to the cathode surface, q_p, and the density of radiation losses of energy by the cathode surface: $q = q_p - \varepsilon\sigma T_w^4$, where ε is the emissivity of the cathode material (a known function of the surface temperature T_w) and σ is the Stefan–Boltzmann constant.

It is assumed that q_p and the density j of electric current from the plasma to the cathode surface are functions of the local temperature T_w of the cathode surface and of the near-cathode voltage drop U: $q_p = q_p(T_w, U)$, $j = j(T_w, U)$. (One of the conditions of validity of this assumption is that the energy flux coming from the arc plasma to the current-collecting part of the cathode surface be generated in a thin near-cathode plasma layer which is independent of the bulk plasma.) The near-cathode voltage drop U is assumed to be a given parameter which is the same at all points of the current-collecting part of the surface.

Under the above assumptions, the boundary condition at the part of the cathode surface that is in contact with the arc plasma and with the cold gas reads

$$\kappa \frac{\partial T}{\partial n} = q(T_w, U), \tag{5}$$

where n is a direction locally orthogonal to the cathode surface and directed outside the cathode.

In the framework of the above approach, a description of the arc–cathode interaction may be constructed in two steps. At the first step, the (one-dimensional) problem describing the current transfer across the near-cathode plasma layer is solved and all parameters of the layer are determined as functions of T_w and U. In particular, densities of the energy flux and of the electric current from the plasma to the current-collecting part of the cathode surface, $q_p = q_p(T_w, U)$ and $j = j(T_w, U)$, are determined. At the second step, the nonlinear thermal-conduction problem (3)–(5) is solved.

A detailed presentation of the model of nonlinear surface heating can be found, e.g. in [7]. Here, we emphasize, what is specified in the framework of this approach is not a distribution of the energy flux from the plasma over the cathode surface but rather a dependence of the energy flux density on the local surface temperature, this temperature being unknown *a priori*. On solving the thermal-conduction problem (3)–(5), one will have complete information on a temperature distribution in the cathode and also on a distribution of the energy flux and electric current over the cathode surface. Integrating the latter, one will find the arc current I corresponding to a value of U being considered.

At present, the second step of the above procedure in most cases does not pose major difficulties, at least as far as solutions describing the diffuse mode of current transfer are concerned. The first step is described in the following section.

Appendix A.2. Near-cathode layer of plasmas composed of atoms of a single species, ions of a single species and electrons

The near-cathode plasma layer comprises a number of sub-layers, of which the most important are a space-charge sheath, which is adjacent to the cathode surface, and an ionization layer, which is adjacent to the sheath. The ion flux to the cathode is generated in the ionization layer. In the sheath, the ions going to the cathode, and electrons emitted from the cathode, are accelerated.

The space-charge sheath is considered collisionless for ions. The number density of the flux of ions to the cathode surface, being equal to the density of flux of ions from the ionization layer to the sheath edge, is evaluated as

$$J_i = n_{is} v_s, \qquad v_s = \sqrt{\frac{k(T_h + T_e)}{m_i}}, \tag{6}$$

where n_{is} is the ion (or electron) density at the sheath edge, v_s is the Bohm velocity, T_e is the temperature of electrons which is assumed to be constant across the ionization layer and the sheath, T_h is the temperature of heavy particles (ions and neutral atoms) which is assumed to be constant across the ionization layer and the sheath and equal to the temperature T_w of the cathode surface and m_i, m_a and m_e here and further are masses of the ion, the atom and the electron.

The number density of flux of plasma electrons which come to the cathode surface from the ionization layer after having overcome the retarding electric field in the space-charge sheath is

$$J_e = \frac{1}{4} n_{is} \sqrt{\frac{8kT_e}{\pi m_e}} \exp\left(-\frac{eU_D}{kT_e}\right), \tag{7}$$

where U_D is the voltage drop in the sheath.

J_{em}, the electron emission flux from the cathode surface, is evaluated by means of the Richardson–Schottky formula. The electric field at the cathode surface, involved in this formula, is obtained by solving the Poisson equation in the sheath jointly with a kinetic equation describing the motion of ions and the

Boltzmann distribution for plasma electrons (the space-charge of emitted electrons is neglected) and reads

$$E_w = \sqrt{\frac{2n_{is}kT_h}{\epsilon_0}}\left[\frac{v_+^3 - v_-^3}{6u_i^3} - \frac{4}{3} - 2\beta + \beta\exp\left(-\frac{eU_D}{kT_e}\right)\right]^{1/2}, \tag{8}$$

where

$$u_i = \sqrt{\frac{kT_h}{m_i}}, \quad \beta = \frac{T_e}{T_h}, \quad v_\pm = \left[(v_s \pm u_i)^2 + \frac{2eU_D}{m_i}\right]^{1/2}. \tag{9}$$

The densities of net electric current and of plasma-related net energy flux to the cathode surface are

$$j = e(J_i + J_{em} - J_e), \qquad q_p = jU - \frac{j}{e}(A + 3.2kT_e). \tag{10}$$

On the edge (plasma side) of the ionization layer, the ionization equilibrium is assumed. The local ion (or electron) density $n_{i\infty}$ and atomic density $n_{a\infty}$ are evaluated, for given temperatures T_h and T_e and plasma pressure p, with the use of the Saha equation. The variation of the charged particle density across the ionization layer is given by the formula

$$\frac{n_{is}}{n_{i\infty}} = \frac{\alpha C_2\sqrt{1+\beta}}{C_2 + 2\alpha C_2\sqrt{1+\beta} + \alpha^2\sqrt{1+\beta}}. \tag{11}$$

Here C_2 is a dimensionless coefficient defined by equation (37) of [28], which depends on β and $\gamma = n_{i\infty}/n_{a\infty}$ and varies for $\beta \geqslant 1$ between approximately 0.67 and 1 (see figure 7 of [23]). α is the ratio of the ionization length to the mean free path for ion–atom collisions defined by the formula [23]

$$\alpha = \sqrt{\frac{2}{3}\frac{C_{ia}Q_{ia}}{k_i}}, \qquad C_{ia} = \sqrt{\frac{8kT_h}{\pi}\left(\frac{1}{m_i} + \frac{1}{m_a}\right)}, \tag{12}$$

where Q_{ia} and k_i are the average cross-section for momentum transfer in elastic ion–atom collisions and the rate constant of ionization of atoms for the gas being considered. Note that C_{ia} has the meaning of average relative speed of ions and atoms; in the case of a plasma produced in a pure monoatomic gas being under consideration in this appendix, $m_i \approx m_a$ and the second equation in equation (12) coincides with the corresponding expression in [23].

The voltage drop in the ionization layer and the total voltage drop in the near-cathode layer are evaluated as

$$U_i = \frac{kT_e}{e}\ln\frac{n_{i\infty}}{n_{is}}, \qquad U = U_D + U_i. \tag{13}$$

The equation of balance of the electron energy in the ionization layer reads

$$J_{em}(2kT_w + eU_D - \Delta A) + \frac{e(J_{em} - J_e) + j}{2}U_i = J_e(2kT_e + eU_D - \Delta A) + 3.2\frac{j}{e}kT_e + J_iE, \tag{14}$$

where ΔA is the Schottky correction to the work function and E is the ionization energy.

The above-described relationships represent a complete set of equations which allows one to determine all parameters of the near-cathode plasma layer for a given plasma-producing gas, plasma pressure and work function of the cathode material as functions of T_w and U. In particular, one can determine functions $q_p(T_w, U)$ and $j(T_w, U)$. A detailed presentation of the model can be found in [7, 9, 18].

References

[1] Benilov M S 1998 *Phys. Rev.* E **58** 6480–94

[2] Coulombe S 2000 *53rd Gaseous Electronics Conf.* (Melville: American Physical Society) *Bull. Am. Phys. Soc.* **45** 18

[3] Krücken T 2001 *Proc. 9th Int. Symp. on Science and Technology of Light Sources (Cornell University, Ithaca, 2001)* ed R S Bergman (Ithaca: Cornell University Press) pp 267–8

[4] Bötticher R and Bötticher W 2001 *J. Phys. D: Appl. Phys.* **34** 1110–5

[5] Graser W 2001 *Proc. 9th Int. Symp. on Science and Technology of Light Sources (Cornell University, Ithaca, 2001)* ed R S Bergman (Ithaca: Cornell University Press) pp 211–2

[6] Bötticher R and Bötticher W 2001 *Proc. 9th Int. Symp. on Science and Technology of Light Sources (Cornell University, Ithaca, 2001)* ed R S Bergman (Ithaca: Cornell University Press) pp 207–8

[7] Benilov M S and Cunha M D 2002 *J. Phys. D: Appl. Phys.* **35** 1736–50

[8] Benilov M S and Cunha M D 2003 *J. Phys. D: Appl. Phys.* **36** 603–14

[9] Benilov M S and Cunha M D 2003 *Phys. Rev.* E **68** 056407

[10] Bötticher R, Graser W and Kloss A 2004 *J. Phys. D: Appl. Phys.* **37** 55–63

[11] Dabringhausen L 2004 Characterization of electrodes of high-pressure plasma lamps by means of pyrometry and simulation *PhD Thesis* Tenea Verlag, Berlin (in German)

[12] Galvez M 2004 *Proc 10th Int. Symp. on Science and Technology of Light Sources (Toulouse, 2004)* ed G Zissis (Bristol: Institute of Physics Publishing) pp 459–60

[13] Luijks G M J F, Nijdam S and Esveld H A V 2004 *Proc. 10th Int. Symp. on Science and Technology of Light Sources (Toulouse, 2004)* ed G Zissis (Bristol: Institute of Physics Publishing) pp 605–6

[14] Lichtenberg S, Dabringhausen L, Mentel J and Awakowicz P 2004 *Proc. 10th Int. Symp. on Science and Technology of Light Sources (Toulouse, 2004)* ed G Zissis (Bristol: Institute of Physics Publishing) pp 609–10

[15] Paul K C, Erraki A, Takemura T, Hiramoto T, Dawson F, Rouffet J B, Gonzalez J J, Gleizes A and Lavers D 2004 *Proc. 10th Int. Symp. on Science and Technology of Light Sources (Toulouse, 2004)* ed G Zissis (Bristol: Institute of Physics Publishing) pp 491–2

[16] Jüttner B 2001 *J. Phys. D: Appl. Phys.* **34** R103–23

[17] Lister G G, Lawler J E, Lapatovich W P and Godyak V A 2004 *Rev. Mod. Phys.* **76** 541–98

[18] Benilov M S and Marotta A 1995 *J. Phys. D: Appl. Phys.* **28** 1869–82

[19] Nandelstädt D, Redwitz M, Dabringhausen L, Luhmann J, Lichtenberg S and Mentel J 2002 *J. Phys. D: Appl. Phys.* **35** 1639–47

[20] http://www.arc_cathode.uma.pt

[21] Almeida R M S, Benilov M S and Naidis G V 2000 *J. Phys. D: Appl. Phys.* **33** 960–7
[22] Biberman L M, Vorob'ev V S and Yakubov I T 1987 *Kinetics of Nonequilibrium Low-Temperature Plasma* (New York: Plenum)
[23] Benilov M S and Naidis G V 1998 *Phys. Rev.* E **57** 2230–41
[24] Voronov G S 1997 *At. Data Nucl. Data Tables* **65** 1–35
[25] Benilov M S, Cunha M D and Naidis G V 2005 *J. Phys. D: Appl. Phys.* **38** at press
[26] Lichtenberg S, Nandelstädt D, Dabringhausen L, Redwitz M, Luhmann J and Mentel J 2002 *J. Phys. D: Appl. Phys.* **35** 1648–56
[27] Thouret W, Weizel W and Günther P 1951 *Z. Phys.* **130** 621–31
[28] Benilov M S 1995 *J. Phys. D: Appl. Phys.* **28** 286–94